ACS Catalysis

Research Article

Cite This: ACS Catal. 2019, 9, 3792−3799

pubs.acs.org/acscatalysis

# Mechanism of Palladium(II)-Mediated Uncaging Reactions of Propargylic Substrates

Sara E. Coelho,[†] Felipe S. S. Schneider,[†] Daniela C. de Oliveira,[‡] Guilherme L. Tripodi,[§] Marcos N. Eberlin,[§] Giovanni F. Caramori,[†] Bernardo de Souza,[†] and Josiel B. Domingos*[,†]

[†]Department of Chemistry, Federal University of Santa Catarina - UFSC, Campus Trindade, C.P. 476, Florianópolis, Santa Catarina 88040-900, Brazil

[‡]Brazilian Synchrotron Light Laboratory, LNLS, C.P. 6192, Campinas, São Paulo 13083-970, Brazil

[§]Thomson Mass Spectrometry Laboratory, University of Campinas-UNICAMP, Campinas, São Paulo 13083-872, Brazil

Supporting Information

**ABSTRACT:** The palladium(II)-mediated chemical uncaging reaction of propargylic substrates is a recent addition to the field of chemical biology and medicinal chemistry in the activation of bio and prodrug molecules. Most of the strategies used involve C−O bond breaking in molecules bearing protected amino and hydroxyl groups. Although this reaction has been known for many decades, its catalytic cycle in aqueous milieu remains unclear. Our mechanistic investigation results unveil that full propargylic substrate conversion occurs through biphasic kinetics of different rates, where the fastest reaction phase involves a Pd(II) anti-Markovnikov hydration of the propargyl moiety, followed by the C−O bond breaking through a $\beta$-O elimination and lasts only for two turnovers due to product inhibition. The second slower reaction phase involves the hydrolysis of the substrate promoted by Pd(0) species formed during the first phase of the reaction. These findings are crucial for the potential development of bioorthogonal Pd catalysts for the uncaging of propargylic protected bioactive and drugs molecules.

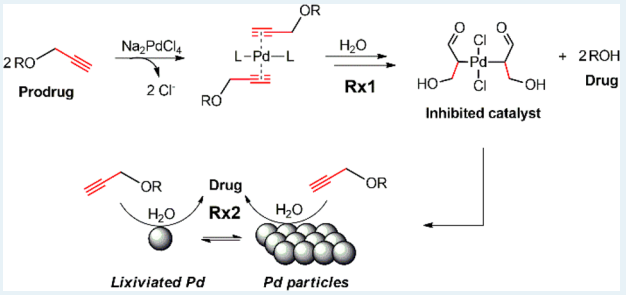


**KEYWORDS:** *depropargylation reaction, palladium, mechanism, catalysis, hydrolysis*

## 1. INTRODUCTION

The promotion of C−O bond cleavage by transition metals is one of the key strategies recently described for uncaging protected molecules possessing hydroxyl and amino functional groups under biocompatible conditions, extra- or intracellularly.[1,2] In particular, palladium-mediated bond-cleavage reactions have gained great interest owing to their unique catalytic properties.[3−8] Cell-surface engineering[9] and protein[10,11] and prodrug[5,12−15] activation outside or inside living cells, through the C−O bond cleavage of propargylic ethers, carbamates, and carbonates (Figure 1a), are examples of the recent applications of palladium-mediated uncaging reactions, taking advantage of a bioorthogonal approach.[16,17] Although it has been argued that carbamate groups are not truly bioorthogonal because they can be deprotected in vivo through the reaction with various nucleophiles and digestive enzymes, propargylic amines and ethers, while less reactive, are more suitable for in vivo applications.[18] Deallylation reactions are also a common strategy, although they are less efficient with simple palladium catalysts than depropargylation.[10] Whereas the mediation of deallylation by Pd(0) through a $\pi$-allylpalladium mechanism is well established,[19] the Pd-mediated depropargylation reaction mechanism remains challenging in the current stage, and no systematic mechanistic studies have been performed.[16] However, it has been most frequently postulated that even when the initial forms of the catalyst are simple Pd(II) salts, the depropargylation reaction mechanism involves the in situ formation of the catalytic species Pd(0). This process is normally assumed to be promoted by a base through an intramolecular ligand exchange reduction or by an attack of a nucleophilic solvent, followed by a reductive elimination pathway.[10−13,16,20−23] The Pd(0) is then assumed to undergo an oxidative addition with the propargyl group to form an allenylpalladium intermediate, which can be hydrolyzed to produce acetol as a side product and to regenerate the Pd(0) (pathway (**i**), Figure 1b). The less common hypothesis is a Pd(II)-mediated hydration mechanism (pathway (**ii**)) to form an intermediate that can decompose to form Pd(II) by hydrolysis (**iii**) in a Wacker-like oxidation.[10,16,24]

However, these uncaging reactions are reported to be relatively slow and present low product yields, requiring high doses of catalyst. The catalyst solubility and toxicity therefore need to be considered when designing a bioorthogonal

Received: January 16, 2019
Revised: February 28, 2019
Published: March 21, 2019






DOI: 10.1021/acscatal.9b00210
ACS Catal. 2019, 9, 3792−3799

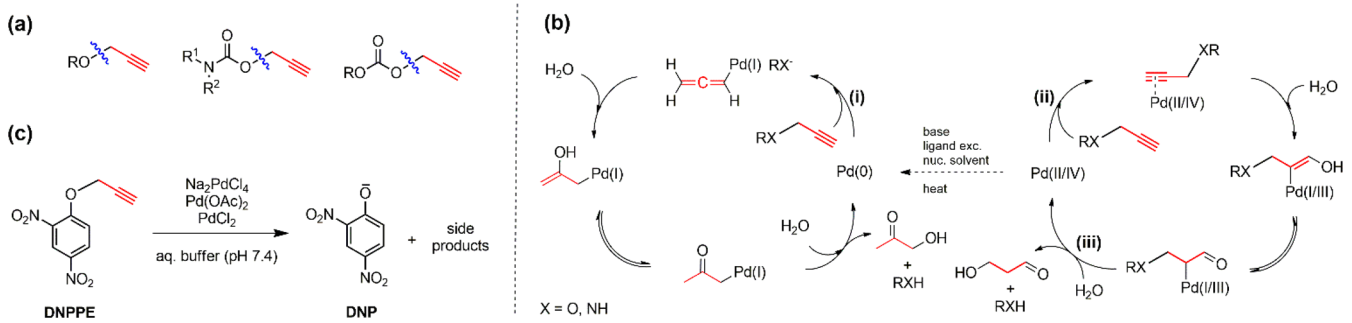


**Figure 1.** (a) Representative examples of C−O bond cleavage of propargyl protected hydroxyl and amino groups. (b) As suggested in the literature, the mechanism for the depropargylation reaction is mediated by Pd(0) (pathway **i**) and Pd(II/IV) (pathway **ii**). (c) Proposed model reaction for the mechanistic studies in this work: prodrug DNPPE uncaging reaction in a phosphate-buffered aqueous medium (pH 7.4) mediated by simple Pd(II) salts.

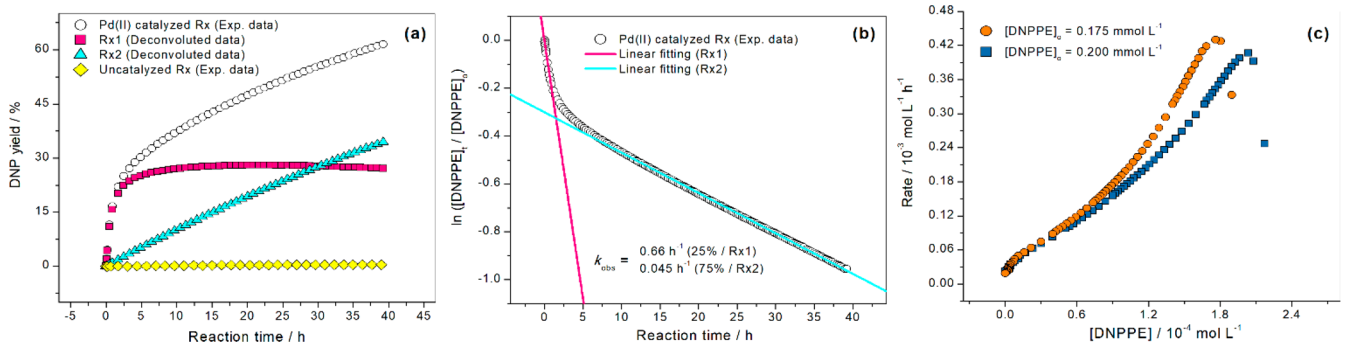


**Figure 2.** (a) Kinetics profiles of product conversion. (b) Natural log of the normalized experimental kinetic data for the DNPPE depropargylation reaction. (c) RPKA of on-cycle catalyst stability during the conversion of DNPPE (experiment 1: $[DNPPE]_0$ = 0.2 mmol $L^{-1}$, $[Pd]_0$ = 0.05 mmol $L^{-1}$ and experiment 2: $[DNPPE]_0$ = 0.175 mmol $L^{-1}$, $[Pd]_0$ = 0.05 mmol $L^{-1}$).

protocol.[25] Thus rational designs of highly elaborate transition-metal catalysts for uncaging reactions will rely on the understanding of fundamental organometallic mechanistic pathways, which can be achieved via both experiments and theoretical calculations to determine the coordination and reaction behavior of reactive intermediates.[26]

In this article, we investigated the mechanism of the C−O bond-cleavage reaction of propargyl protected hydroxyl groups, triggered by the addition of simple Pd(II) salts ($Na_2PdCl_4$, $Pd(OAc)_2$, and $PdCl_2$), without the addition of base or ligands, in phosphate-buffered aqueous medium (pH 7.4). The prodrug compound 2,4-dinitrophenyl propargyl ether (DNPPE) was chosen as a model substrate for these studies (Figure 1c). DNPPE is a caged protonophore that becomes an active mitochondrial uncoupler (DNP)[27] after the removal of the propargyl protecting group. DNP is a widely studied pharmacological uncoupling agent used in experimental models of neurodegenerative conditions.[28−30] Moreover, DNP is a tyrosine analogue, a catalytic residue present in many enzymes, and consequently a model compound for the bioconjugation of proteins.[11,31] Also, the deprotection yield of DNPPE can be linked directly to UV−vis spectroscopy readouts, which offers a simple approach for an assessment of the reaction progress.

## 2. RESULTS AND DISCUSSION

In phosphate-buffered aqueous medium (pH 7.4), the reactions mediated by the Pd(II) salts were monitored by UV−vis spectroscopy through the appearance of the product DNP at a wavelength of 400 nm (Figure S1). For all Pd(II) salts, a deviation from the first-order kinetics was observed (open circles, Figure 2a, for the reaction mediated by $Na_2PdCl_4$ and Figure S2 for the other salts). The distinct biexponential shape of the curve is not consistent with a simple reaction mechanism. Indeed, these profiles were typical of biphasic kinetics, producing the same product (DNP) at different rates (eq 1).[32,33] The linear fit of eq 1 enabled the determination of two observed macroscopic rate constants ($k_1$ and $k_2$, Figure 2b).

$$\frac{[DNPPE]_t}{[DNPPE]_0} = F^0 e^{-k_1 t} + S^0 e^{-k_2 t} \quad (1)$$

The yield magnitudes of the fast ($k_1$) and slow ($k_2$) phases are denoted by $F^0$ (25%) and $S^0$ (75%), respectively. On the basis of these macroscopic rate constants, the evolution of the DNP product was deconvoluted into two reaction kinetics profiles (Figure 2a, red squares and blue triangles for the fast and slow phases, respectively), namely, Rx1 and Rx2, respectively. It can be observed that Rx1 was ∼15 times faster than Rx2 ($k$ = 0.66 and 0.045 $h^{-1}$, respectively) and ∼650 times faster than the uncatalyzed reaction ($k_{unc}$ = 1.02 × $10^{-3}$ $h^{-1}$) under the same conditions. The half life for Rx1 is ∼1 h, which makes this reaction feasible for bioorthogonal applications.[34]

It is important to note that the fast phase (Rx1) is responsible for the conversion of ∼20 mol % into the product DNP, that is, only two turnovers (Figure S3). Mechanistically, this information shows that although Rx1 is faster than Rx2, it shuts down after two turnovers. In fact, sequential addition of the catalyst after different reaction times leads to a sharp increase in the DNP production, which also lasts for around



DOI: 10.1021/acscatal.9b00210
ACS Catal. 2019, 9, 3792−3799

two turnovers (Figure S4). We found this to be very important because for many of the Pd catalysts reported herein, the reaction was monitored during a short period, and the turnover, especially intracellularly, was not properly established.[17]

For a single-substrate catalytic cleavage reaction, a biphasic time course is consistent with a change in mechanism owed to a change in the activity of the catalyst. Thus an experiment by reaction progress kinetic analysis (RPKA) was performed to establish catalyst stability over the entire reaction course. RPKA can suggest a few initial sets of experiments to find any evidence of catalyst deactivation or product inhibition.[35] Therefore, two reactions initiated with different initial concentrations of DNPPE and the same catalyst concentration should display identical rate versus substrate concentration profiles in the absence of catalyst deactivation or product inhibition processes. Consequently, two reactions were performed: experiment 1 with $[DNPPE]_0$ = 0.2 mmol $L^{-1}$ and experiment 2 with $[DNPPE]_0$ = 0.175 mmol $L^{-1}$ (Figure 2c). Figure 2c shows an unmatched rate behavior through the graphical overlay, suggesting that [Pd] is unequal for both experiments. These results indicate that the catalyst is not stable, which is further supported by later experiments revealing that the catalyst is changing to accommodate a switch in the mechanism. Moreover, further kinetic experiments adding DNP or acetol (the most frequently reported byproduct for this reaction) to the reaction medium show that neither affects the reaction profile (Figure S5). Thus a possible inhibition due the presence of DNP or possibly acetol products is ruled out.

Other parameters can also influence the reaction rate; for instance, increasing the Pd concentration from 2 to 12 mol % of Pd(II) resulted in an increase in the reaction rate by factors of 10 for Rx1 and 45 for Rx2 (Figure S6). The nonlinear response of Rx1/Rx2 reaction rates with changes in Pd concentration suggests a different nuclearity in the catalyst for these two processes. The phosphate buffer concentration also altered the reaction rate for Rx1, with a decrease observed from 0.01 to 0.15 mol $L^{-1}$, but it had no effect in the case of Rx2 (Figure S7). The amount of cosolvent DMSO affected the reaction rate as well; an increase from 10 to 50% of DMSO almost completely inhibited both reactions (Figure S8). This is important because DMSO is by far the most common cosolvent used in these reactions for substrate solubilization in aqueous solution in vitro or in vivo experiments. Because of the known coordination capabilities of phosphate and DMSO toward transition metals, the concentrated buffer and cosolvent are probably inhibiting the reaction through complexation with the catalytic species. The stronger inhibition effect of the buffer in the case of Rx1 shows that the Pd species involved in this reaction is a more labile one.

As discussed before, the most general assumption in the literature is that this reaction mechanism occurs via oxidative addition of the propargyl C−O bond to Pd(0) (Figure 1b, pathway **i**). Thus to investigate the true nature of the catalytic species, we tested the hypothesis that the involvement of Pd(0) formed spontaneously from the reduction of Pd(II) in the reaction medium. First, we performed X-ray absorption spectroscopy (XAS) analysis of the reaction medium after 3 h under the same conditions used during the standard reaction (buffered aqueous medium, pH 7.4, at 48 °C) but without the addition of substrate. The $Na_2PdCl_4$ salt was chosen due to its higher solubility in water, and the XAS data were collected on a synchrotron-based setup in transmission mode at the Pd−K edge (24.35 keV). (See the Supporting Information for details of the XAS setup.) As shown in Figure S9, the extended X-ray absorption fine structure (EXAFS) fitting results show an intense Pd(II)−Cl bond signal and the absence of the Pd(0)−Pd(0) or Pd(II)−O bond signals, which would be observed if Pd(0) species or Pd(II) hydrolysis products had been formed in the reaction medium during the 3 h of the experiment.[36,37] It is clear from these results that under these reaction conditions, no Pd(0) is spontaneously formed, but we do not rule out the possible formation of Pd(0) in the presence of the substrate, for example, due to a Wacker-type reaction. The nature of the catalysts in the presence of substrate was not investigated by XAS due to the low solubility of DNPPE.

Thus two mechanistic scenarios could possibly act in the faster kinetic phase. If Pd(0) was somehow formed in the presence of substrate, then the reaction would occur via an oxidative addition at the propargyl group, or the other scenario would be a hydration of the propargyl group coordinated to a Pd(II) (Figure 1b, pathways **i** and **ii**, respectively). To distinguish between these possible pathways, we have performed a kinetic experiment adding $CS_2$ at 0 h and after 2 h of reaction time. $CS_2$ acts as a catalyst poison for homogeneous and heterogeneous Pd(0) catalysts at temperatures below 50 °C, whereas Pd(II) species are unaffected.[38] As show in Figure S10, the initial reaction rate for the faster phase in all cases is similar. This result indicates that there is no participation of Pd(0) species in the faster phase (Rx1). On the contrary, the slower phase (Rx2) rate has been intensely affected by the addition of $CS_2$, most probably due the participation of Pd(0) in this reaction phase.

Continuing with the aim to unveil the nature of the catalytic species, high-resolution electrospray ionization mass spectrometry (ESI−HRMS) was used to monitor the reaction and possible detection of key reaction intermediates.[39−42] ESI is a soft ionization technique that can be used to analyze both cations and anions, displays high sensitivity, and allows the immediate transfer to the gas phase of most ionic species present in the reaction solution. Working in negative ion mode, the in situ ESI(−)−HRMS monitoring of the reaction, with 20 mol % of $Na_2PdCl_4$ in phosphate-buffered aqueous solution pH 7.4 (5% DMSO) provided 10 min after the start of the reaction, identified the following proposed species: the product DNP ($m/z$ = 183) as the major species (Figure 3a) and three other Pd species interacting with the substrate at $m/z$ 434.8, 416.9, and 638.9 (Figure 3b−d). The species at $m/z$ 434.8 (**1**, Figure 3b) is a $\pi$ complex of $PdCl_3$ with DNPPE, and the Pd signal at $m/z$ 416.9 may be one of the several possible carbopalladate isomers formed from the hydration (Markovnikov or anti-Markovnikov) of the $\pi$ complex [DNPPE−$PdCl_3$] (**2**, Figure 3c). We shall see later that computational calculations revealed that the ketone isomer is more stable (∼16 kcal $mol^{-1}$).

The third species identified is a hydrolyzed (Markovnikov or anti-Markovnikov) carbopalladate intermediate complexed with another DNPPE molecule through a $\pi$ interaction (**3**, Figure 3d). The agreement between the experimental and calculated (Figure S11) isotopologue patterns and exact masses corroborates the proposed structures and elemental compositions. Moreover, the ESI−HRMS analysis after 35 min of reaction shows that species **1** and **2** are still present, but after 120 min, only the DNP product can be observed. In addition, the analysis of a precipitate formed after 35 min of reaction



DOI: 10.1021/acscatal.9b00210
ACS Catal. 2019, 9, 3792−3799

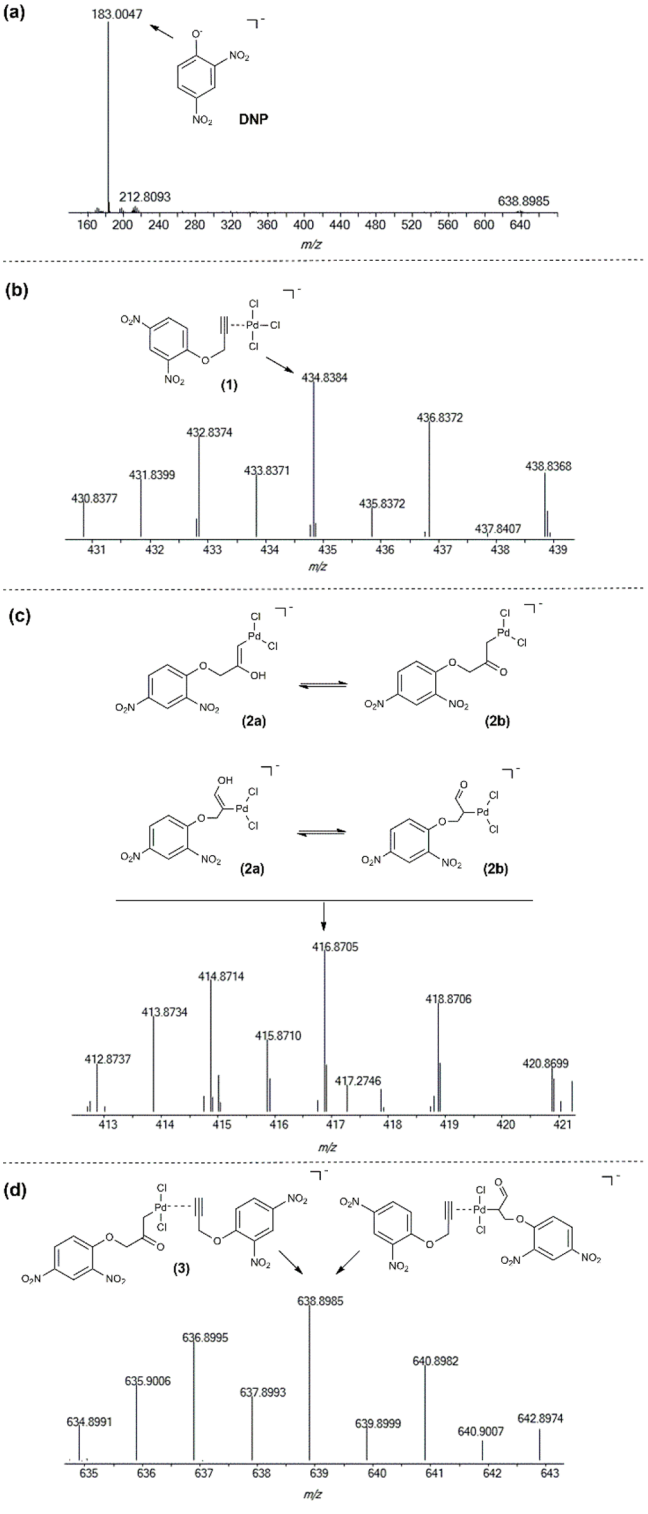


**Figure 3.** ESI(−)−HRMS of the reaction medium 10 min after the start of the DNPPE depropargylation reaction. The ions at $m/z$ 434.8 (b), $m/z$ 416.9 (c), and $m/z$ 638.9 (d) were detected in lower abundance compared with the product ion DNP (a), so the spectral regions of interest were amplified ([DNPPE] = 2.12 mmol $L^{-1}$, [$Na_2PdCl_4$] = 20 mol %, in $H_2O$ (5% DMSO), pH 7.4 at 48 °C).

also identified an ion at $m/z$ 473 (Figure S12), corresponding to another hydrolyzed carbopalladate intermediate. Ion **3** was then further characterized by ESI collision-induced dissociation tandem mass spectrometry (ESI−CID−MS/MS). The observed fragmentation pathways of these reaction intermediates reflect their intrinsic reactivity and support the proposed structures of **3**. (See Figure S13 for further discussion.)

These species identified by ESI−HRMS, together with the results from the kinetic studies, align more with an alkyne hydration pathway than with an oxidative addition pathway, at least for the initial part of the reaction, that is, for the faster reaction phase. To explore the details of the fast Rx1 and possibly exploit it in the future, we also performed computational studies. On the basis of the XAS results, the complex $[PdCl_4]^{2-}$ was used as the catalyst species, and we chose the model substrate methyl−propargyl ether to simplify the calculations. All simulations were performed with an implicit solvent model, and we added two extra water molecules to consider the effect of explicit solvation, one interacting with the enol part and the other interacting with the leaving group. Geometries and frequencies were calculated with the functional PBE0,[43] and, to obtain very accurate energetics, DLPNO−CCSD(T)[44] was used to compute the energies, and the HF-gCP[45] correction was added to minimize basis set artifacts.

Surprisingly, the energy difference between the Markovnikov and anti-Markovnikov regiochemical hydrations of the Pd−propargyl complex to form enols is low (<1 kcal $mol^{-1}$), falling within the error of the method (Figure S14). Thus both pathways to product formation were explored. After the formation of the enol, a tautomerization can occur (also suggested by ESI−HRMS, Figure 3c), and we found that keto tautomers are the most stable. Next, we searched for the C−O bond break step for both regiochemical keto tautomer intermediates. For the anti-Markovnikov keto intermediate (**$C_2$**, Figure S14), the first-expected $S_N2$-like hydrolysis is not much faster than the uncatalyzed reaction, with the transition state being stabilized by only ca. 8 kcal $mol^{-1}$. We then searched for other mechanistic pathways, such as an intramolecular attack of the oxygen ($\Delta G^{\ddagger}$ = 58.7 kcal $mol^{-1}$), $\beta$-H elimination of Pd, followed by hydrolysis (this pathway was discarded due the high acidity of methylene H) and concluded that a $\beta$-O elimination mechanism was most likely, with the C−O bond breaking prior to a subsequent attack of water ($\Delta G^{\ddagger}$ = 38 kcal $mol^{-1}$). For the Markovnikov keto intermediate (**$C_2'$**, Figure S14), the $S_N2$-like hydrolysis presented much higher activation energy ($\Delta G^{\ddagger}$ = 54.02 kcal $mol^{-1}$) than the $\beta$-O elimination of the anti-Markovnikov keto intermediate. The complete calculation for the first reaction turnover of the main mechanism is depicted in Figure 4.

Thus we propose that the most probable operating reaction pathway for Rx1 involves the coordination of DNPPE molecules to Pd(II), followed by an anti-Markovnikov attack of water molecules at the propargyl moiety, prior to the C−O bond breaking by $\beta$-O elimination and hydration (Figure 5). The proposed pathways for Rx1 shown in Figure 5 involve the stepwise C−O bond cleavages (**2** → **4** → **5** → **6** → **7** → **8**). In this scenario, the final products are two equivalents of DNP and the bis(1-hydroxy-3-oxopropan-2-yl)palladium(II) chloride, the carbopalladate complex **8**. Although the formation of **8** could not be confirmed by analytical tools such as ESI−HRMS or even by $H^1$ NMR (Figure S15), its existence is supported by the detection of only two turnovers during Rx1 because the binding of a third DNPPE molecule is less likely due to steric hindrance.

The $K_{eq}$ values calculated for two insertions of the propargyl ether substrate are 4.9 × $10^{-4}$ for the first and 6.3 × $10^{-4}$ for



DOI: 10.1021/acscatal.9b00210
ACS Catal. 2019, 9, 3792−3799

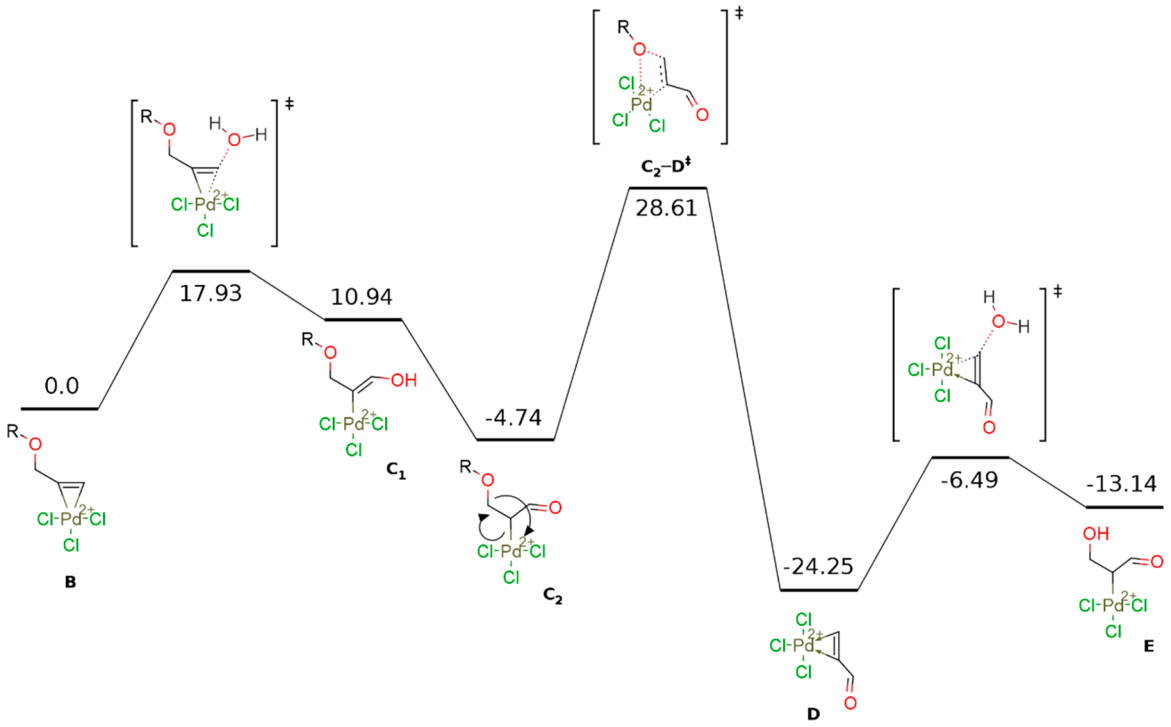


**Figure 4.** Energy profile (kcal mol$^{-1}$) calculated for the first turnover of the depropargylation reaction catalyzed by $[PdCl_4]^{2-}$ in water.

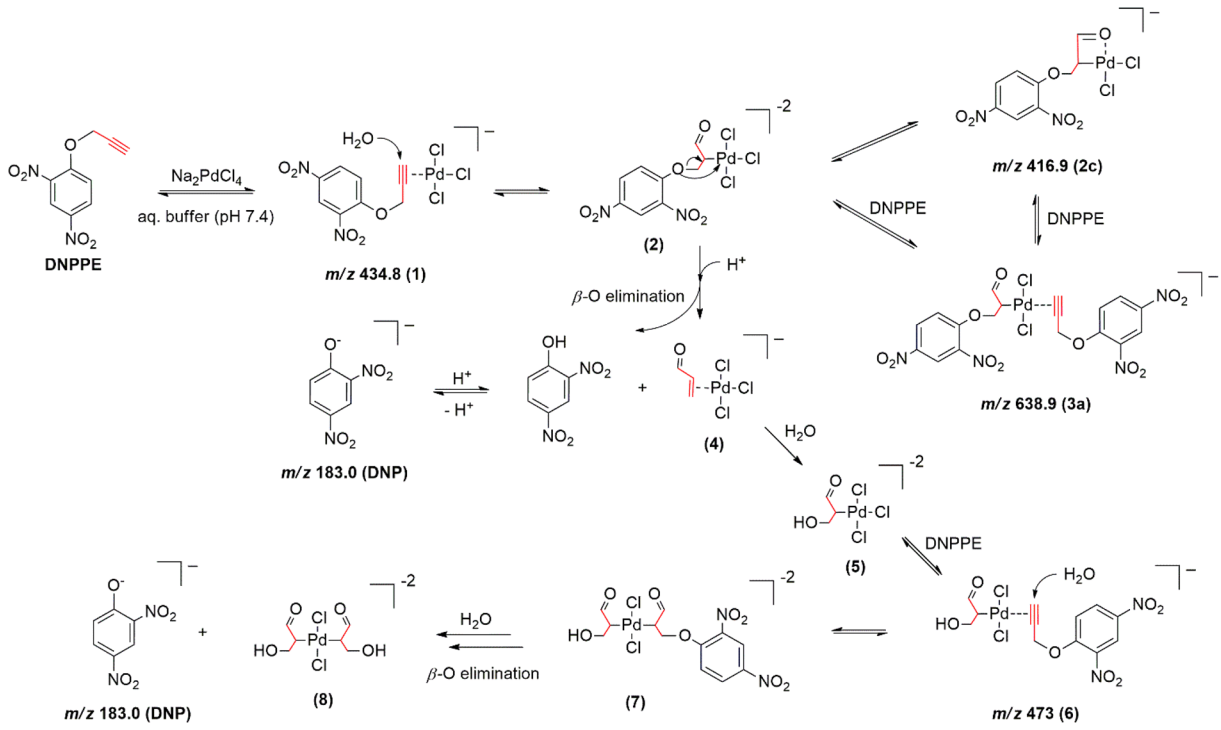


**Figure 5.** Proposed pathways for Rx1 in the depropargylation reaction of DNPPE mediated by Pd(II) salts.

the second insertion, but the binding of a third molecule, displacing a chloride, has a constant of $7.6 \times 10^{-8}$ (Figure S14) and probably does not happen at all; in this case, complex **8** can be considered a product-inhibited Pd catalyst. Indeed, when 50 mol % of Pd is used, the quantitative formation of DNP is reached in <2 h in a monophasic first-order kinetic profile (Figure S16) for all three Pd(II) salts used in this study. As can be seen, the role of the metal in this first step is two-fold: It facilitates the hydration of the triplet bond and stabilizes the keto tautomer intermediate during the C−O bond breaking. We assume that when a second substrate is coordinated, the same hydrolytic mechanism is followed.

To test the hypothesis of complex **8** formation, we added propargyl alcohol in the reaction medium and waited for 2 h before the addition of the substrate. The idea is that under this time, the propargyl alcohol, complexed with Pd(II), would be



DOI: 10.1021/acscatal.9b00210
ACS Catal. 2019, 9, 3792−3799

hydrolyzed and inhibit further complexation of DNPPE molecules. In fact, as shown in Figure S17, Rx1 was much slower with the addition of propargyl alcohol. This result corroborates the proposed mechanism for Rx1.

On the basis of the kinetic evidence and poisoning studies (see below), it is more likely that after these first two turnovers, Rx2 is undergoing a different mechanism. When the reaction was performed with a higher substrate concentration, a dark precipitate was observed after the reaction completion. This precipitate was analyzed by transmission electron microscopy (Figure S18) and synchrotron-based X-ray absorption spectroscopy (XANES/EXAFS) (Figure S19). These experiments revealed the presence of 5 nm Pd nanoparticles (Pd NPs) and palladium with a mixed oxidation state. (See the Supporting Information for further details and discussion.) The reaction was then monitored by dynamic light scattering (DLS, Figure S20), and the presence of nanoparticles (hydrodynamic ratio between 8 and 15 nm) was observed beginning at 5 min of reaction, although in very low concentration.

These observations motivated us to perform further poisoning experiments to determine the catalytically active species for Rx2. Figure S21 shows the reaction kinetic profiles with $CS_2$ and Hg(0) added after 120 min of reaction compared with the reactions without the additives. As discussed before, $CS_2$ acts as a catalyst poison for homogeneous and heterogeneous catalysts,[38] whereas Hg(0) poisons metal-particle heterogeneous catalysts by amalgamating the metal or adsorbing onto the metal surface, especially palladium, with homogeneous complexes remaining unaffected.[46] The addition of $CS_2$ completely inhibits the catalytic activity of Rx2, but the presence of mercury inhibits the DNP formation by ~60%. These results indicate that the catalytic activity of the slower phase of the reaction (Rx2) is mainly a result of Pd(0) NPs formed during the reaction or lixiviated Pd(0) atoms from the NPs (Figure 6); the formation of these Pd(0) species from the Pd(II) complex **8** may explain why this product has not been detect by any analytical tools employed. In fact, when the reaction was performed in the presence of as-synthesized Pd(0) NPs, the reaction was extremely slow (Figure S22), supporting the nature of the Rx2 phase of the reaction.

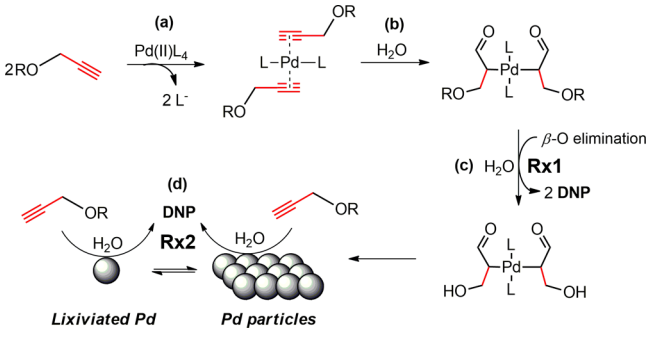


**Figure 6.** Pd(II) catalytic fate in the DNPPE *O*-depropargylation reaction. The full substrate conversion is a consequence of two different catalytic cycles: (**i**) Two equivalents of substrate are converted in a fast reaction, where the initial step is a ligand exchange (a), followed by hydration of the triple bond (b) and C−O bond cleavage by *β*-O elimination, followed by hydration (c). (**ii**) The second and less effective cycle might be the result of a Pd(0) nanoparticles/lixiviated catalytic species formed after the first cycle (d). L = ligand (e.g., $Cl^-$ and $AcO^-$). R = 2,4-dinitrophenyl group.

## 3. CONCLUSIONS

We have shown that simple Pd(II) salts can effectively act as catalysts for the *O*-depropargylation reaction under biocompatible conditions, but the reaction is biphasic, presenting a fast and a slow phase, revealing that the catalyst is changing to accommodate a switch in the mechanism. The faster phase ends after two turnovers due to product inhibition. This explains the frequently reported need for high doses of these catalysts for a fast full conversion of the substrate. The mechanism for the faster phase involves key intermediates where the Pd(II) is inserted with anti-Markovnikov orientation at the propargyl moiety prior to the C−O bond cleavage by a *β*-O elimination, as suggested by theoretical modeling, whereas the slow phase involves the hydrolysis of the substrate promoted by Pd(0) species formed during the first phase of the reaction. These findings will help to design and control the selective reactivity of new palladium catalysts for uncaging reactions of *O*-propargyl substrates, especially discrete Pd complexes.[47] For example, we envision that Pd complexes with bulky ligands may be a better choice for this reaction because the expulsion of the reaction product can be tuned by the steric bulkiness of the ligands, avoiding the inhibition of the catalyst by the reaction product derived from the propargyl moiety. These studies are currently underway in our laboratory.

## ■ ASSOCIATED CONTENT

### Supporting Information

The Supporting Information is available free of charge on the ACS Publications website at DOI: 10.1021/acscatal.9b00210.

Detailed experimental procedures, reaction kinetics profiles, and spectroscopic analysis (PDF)

## ■ AUTHOR INFORMATION

### Corresponding Author

*E-mail: josiel.domingos@ufsc.br.

### ORCID

Sara E. Coelho: 0000-0001-9145-5657
Felipe S. S. Schneider: 0000-0001-8090-2976
Giovanni F. Caramori: 0000-0002-6455-7831
Josiel B. Domingos: 0000-0002-6001-4522

### Notes

The authors declare no competing financial interest.

## ■ ACKNOWLEDGMENTS

We are grateful to CNPq and CAPES for the financial support received for this study. We also thank the Brazilian Synchrotron Light Laboratory (LNLS) team for XAS experiments carried out under proposals 20160243/20170351 on the XDS beamline, using the experimental station developed for the EMA beamline at SIRIUS source, the Central Laboratory of Electron Microscopy (LCME) at UFSC (for the TEM analysis), and the Brazilian National Center for Supercomputing (CESUP/UFRGS). This paper is dedicated in memory of Professor Faruk José Nome Aguilera (1947−2018).

## ■ REFERENCES

(1) Li, J.; Chen, P. R. Development and Application of Bond Cleavage Reactions in Bioorthogonal Chemistry. *Nat. Chem. Biol.* **2016**, *12*, 129−137.

(2) Pérez-López, A. M.; Rubio-Ruiz, B.; Sebastián, V.; Hamilton, L.; Adam, C.; Bray, T. L.; Irusta, S.; Brennan, P. M.; Lloyd-Jones, G. C.;



DOI: 10.1021/acscatal.9b00210
*ACS Catal.* 2019, 9, 3792−3799

Sieger, D.; Santamaría, J.; Unciti-Broceta, A. Gold-Triggered Uncaging Chemistry in Living Systems. *Angew. Chem., Int. Ed.* **2017**, *56*, 12548−12552.
(3) Yusop, R. M.; Unciti-Broceta, A.; Johansson, E. M. V.; Sánchez-Martín, R. M.; Bradley, M. Palladium-Mediated Intracellular Chemistry. *Nat. Chem.* **2011**, *3*, 239−243.
(4) Yang, M. Y.; Li, J.; Chen, P. R. Transition Metal-Mediated Bioorthogonal Protein Chemistry in Living Cells. *Chem. Soc. Rev.* **2014**, *43*, 6511−6526.
(5) Völker, T.; Meggers, E. Transition-Metal-Mediated Uncaging in Living Human Cells — an Emerging Alternative to Photolabile Protecting Groups. *Curr. Opin. Chem. Biol.* **2015**, *25*, 48−54.
(6) Dumas, A.; Couvreur, P. Palladium: A Future Key Player in the Nanomedical Field? *Chemical Science* **2015**, *6*, 2153−2157.
(7) Chankeshwara, S. V.; Indrigo, E.; Bradley, M. Palladium-Mediated Chemistry in Living Cells. *Curr. Opin. Chem. Biol.* **2014**, *21*, 128−135.
(8) Jbara, M.; Maity, S. K.; Brik, A. Palladium in the Chemical Synthesis and Modification of Proteins. *Angew. Chem., Int. Ed.* **2017**, *56*, 10644−10655.
(9) Wang, J.; Cheng, B.; Li, J.; Zhang, Z.; Hong, W.; Chen, X.; Chen, P. R. Chemical Remodeling of Cell-Surface Sialic Acids through a Palladium-Triggered Bioorthogonal Elimination Reaction. *Angew. Chem., Int. Ed.* **2015**, *54*, 5364−5368.
(10) Li, J.; Yu, J.; Zhao, J.; Wang, J.; Zheng, S.; Lin, S.; Chen, L.; Yang, M.; Jia, S.; Zhang, X.; Chen, P. R. Palladium-Triggered Deprotection Chemistry for Protein Activation in Living Cells. *Nat. Chem.* **2014**, *6*, 352−361.
(11) Wang, J.; Zheng, S.; Liu, Y.; Zhang, Z.; Lin, Z.; Li, J.; Zhang, G.; Wang, X.; Li, J.; Chen, P. R. Palladium-Triggered Chemical Rescue of Intracellular Proteins Via Genetically Encoded Allene-Caged Tyrosine. *J. Am. Chem. Soc.* **2016**, *138*, 15118−15121.
(12) Weiss, J. T.; Dawson, J. C.; Macleod, K. G.; Rybski, W.; Fraser, C.; Torres-Sánchez, C.; Patton, E. E.; Bradley, M.; Carragher, N. O.; Unciti-Broceta, A. Extracellular Palladium-Catalysed Dealkylation of 5-Fluoro-1-Propargyl-Uracil as a Bioorthogonally Activated Prodrug Approach. *Nat. Commun.* **2014**, *5*, 3277.
(13) Weiss, J. T.; Dawson, J. C.; Fraser, C.; Rybski, W.; Torres-Sánchez, C.; Bradley, M.; Patton, E. E.; Carragher, N. O.; Unciti-Broceta, A. Development and Bioorthogonal Activation of Palladium-Labile Prodrugs of Gemcitabine. *J. Med. Chem.* **2014**, *57*, 5395−5404.
(14) Tonga, G. Y.; Jeong, Y.; Duncan, B.; Mizuhara, T.; Mout, R.; Das, R.; Kim, S. T.; Yeh, Y.-C.; Yan, B.; Hou, S.; Rotello, V. M. Supramolecular Regulation of Bioorthogonal Catalysis in Cells Using Nanoparticle-Embedded Transition Metal Catalysts. *Nat. Chem.* **2015**, *7*, 597−603.
(15) Stenton, B. J.; Oliveira, B. L.; Matos, M. J.; Sinatra, L.; Bernardes, G. J. L. A Thioether-Directed Palladium-Cleavable Linker for Targeted Bioorthogonal Drug Decaging. *Chemical Science* **2018**, *9*, 4185−4189.
(16) Martínez-Calvo, M.; Mascareñas, J. L. Organometallic Catalysis in Biological Media and Living Settings. *Coord. Chem. Rev.* **2018**, *359*, 57−79.
(17) Bai, Y.; Chen, J.; Zimmerman, S. C. Designed Transition Metal Catalysts for Intracellular Organic Synthesis. *Chem. Soc. Rev.* **2018**, *47*, 1811−1821.
(18) Vinogradova, E. V. Organometallic Chemical Biology: An Organometallic Approach to Bioconjugation. *Pure Appl. Chem.* **2017**, *89*, 1619−1640.
(19) Garner, A. L.; Song, F.; Koide, K. Enhancement of a Catalysis-Based Fluorometric Detection Method for Palladium through Rational Fine-Tuning of the Palladium Species. *J. Am. Chem. Soc.* **2009**, *131*, 5163−5171.
(20) Amatore, C.; Jutand, A.; Thuilliez, A. Formation of Palladium(0) Complexes from Pd(Oac)2 and a Bidentate Phosphine Ligand (Dppp) and Their Reactivity in Oxidative Addition. *Organometallics* **2001**, *20*, 3241−3249.
(21) Pal, M.; Parasuraman, K.; Yeleswarapu, K. R. Palladium-Catalyzed Cleavage of O/N-Propargyl Protecting Groups in Aqueous Media under a Copper-Free Condition1. *Org. Lett.* **2003**, *5*, 349−352.
(22) Rambabu, D.; Bhavani, S.; Swamy, N. K.; Basaveswara Rao, M. V.; Pal, M. Pd/C-Mediated Depropargylation of Propargyl Ethers/Amines in Water. *Tetrahedron Lett.* **2013**, *54*, 1169−1173.
(23) Wei, C. S.; Davies, G. H. M.; Soltani, O.; Albrecht, J.; Gao, Q.; Pathirana, C.; Hsiao, Y.; Tummala, S.; Eastgate, M. D. The Impact of Palladium(Ii) Reduction Pathways on the Structure and Activity of Palladium(0) Catalysts. *Angew. Chem., Int. Ed.* **2013**, *52*, 5822−5826.
(24) Liu, B.; Wang, H.; Wang, T.; Bao, Y.; Du, F.; Tian, J.; Li, Q.; Bai, R. A New Ratiometric Esipt Sensor for Detection of Palladium Species in Aqueous Solution. *Chem. Commun. (Cambridge, U. K.)* **2012**, *48*, 2867−2869.
(25) Sletten, E. M.; Bertozzi, C. R. Bioorthogonal Chemistry: Fishing for Selectivity in a Sea of Functionality. *Angew. Chem., Int. Ed.* **2009**, *48*, 6974−6998.
(26) Murahashi, T.; Ogoshi, S.; Kurosawa, H. New Direction in Organopalladium Chemistry: Structure and Reactivity of Unsaturated Hydrocarbon Ligands Bound to Multipalladium Units. *Chem. Rec.* **2003**, *3*, 101−111.
(27) Chalmers, S.; Caldwell, S. T.; Quin, C.; Prime, T. A.; James, A. M.; Cairns, A. G.; Murphy, M. P.; McCarron, J. G.; Hartley, R. C. Selective Uncoupling of Individual Mitochondria within a Cell Using a Mitochondria-Targeted Photoactivated Protonophore. *J. Am. Chem. Soc.* **2012**, *134*, 758−761.
(28) Wu, B.; Jiang, M.; Peng, Q.; Li, G.; Hou, Z.; Milne, G. L.; Mori, S.; Alonso, R.; Geisler, J. G.; Duan, W. 2,4 Dnp Improves Motor Function, Preserves Medium Spiny Neuronal Identity, and Reduces Oxidative Stress in a Mouse Model of Huntington's Disease. *Exp. Neurol.* **2017**, *293*, 83−90.
(29) Khan, R. S.; Dine, K.; Geisler, J. G.; Shindler, K. S. Mitochondrial Uncoupler Prodrug of 2,4-Dinitrophenol, Mp201, Prevents Neuronal Damage and Preserves Vision in Experimental Optic Neuritis. *Oxid. Med. Cell. Longevity* **2017**, *2017*, 1−10.
(30) Geisler, J. G.; Marosi, K.; Halpern, J.; Mattson, M. P. Dnp, Mitochondrial Uncoupling, and Neuroprotection: A Little Dab'll Do Ya. *Alzheimer's Dementia* **2017**, *13*, 582−591.
(31) Trader, D. J.; Carlson, E. E. Chemoselective Hydroxyl Group Transformation: An Elusive Target. *Mol. BioSyst.* **2012**, *8*, 2484−2493.
(32) Kayastha, A. M.; Gupta, A. K. An Easy Method to Determine the Kinetic-Parameters of Biphasic Reactions. *Biochem. Educ.* **1987**, *15*, 135−135.
(33) Anderson, T. G.; McConnell, H. M. Interpretation of Biphasic Dissociation Kinetics for Isomeric Class Ii Major Histocompatibility Complex-Peptide Complexes. *Biophys. J.* **1999**, *77*, 2451−2461.
(34) Devaraj, N. K. The Future of Bioorthogonal Chemistry. *ACS Cent. Sci.* **2018**, *4*, 952−959.
(35) Blackmond, D. G. Reaction Progress Kinetic Analysis: A Powerful Methodology for Mechanistic Studies of Complex Catalytic Reactions. *Angew. Chem., Int. Ed.* **2005**, *44*, 4302−4320.
(36) Yao, Y.; Patzig, C.; Hu, Y.; Scott, R. W. J. In Situ X-Ray Absorption Spectroscopic Study of Fe@Fexoy/Pd and Fe@Fexoy/Cu Nanoparticle Catalysts Prepared by Galvanic Exchange Reactions. *J. Phys. Chem. C* **2015**, *119*, 21209−21218.
(37) Chang, S. Y.; Grunder, Y.; Booth, S. G.; Molleta, L. B.; Uehara, A.; Mosselmans, J. F. W.; Cibin, G.; Pham, V. T.; Nataf, L.; Dryfe, R. A. W.; Schroeder, S. L. M. Detection and Characterisation of Sub-Critical Nuclei During Reactive Pd Metal Nucleation by X-Ray Absorption Spectroscopy. *CrystEngComm* **2016**, *18*, 674−682.
(38) Charbonneau, M.; Addoumieh, G.; Oguadinma, P.; Schmitzer, A. R. Support-Free Palladium−Nhc Catalyst for Highly Recyclable Heterogeneous Suzuki−Miyaura Coupling in Neat Water. *Organometallics* **2014**, *33*, 6544−6549.
(39) Santos, L. S. In *Reactive Intermediates*; Wiley-VCH Verlag GmbH & Co. KGaA: 2010; pp 133−198.
(40) Roglans, A.; Pla-Quintana, A. In *Reactive Intermediates*; Wiley-VCH Verlag GmbH & Co. KGaA: 2010; pp 229−275.


DOI: 10.1021/acscatal.9b00210
*ACS Catal.* 2019, 9, 3792−3799

(41) Qian, R.; Zhou, J.; Yao, S.; Wang, H.; Guo, Y. In *Reactive Intermediates*; Wiley-VCH Verlag GmbH & Co. KGaA: 2010; pp 113−131.
(42) Nachtigall, F. M.; Eberlin, M. N. In *Reactive Intermediates*; Wiley-VCH Verlag GmbH & Co. KGaA: 2010; pp 63−111.
(43) Adamo, C.; Barone, V. Toward Reliable Density Functional Methods without Adjustable Parameters: The Pbe0Model. *J. Chem. Phys.* **1999**, *110*, 6158−6170.
(44) Riplinger, C.; Sandhoefer, B.; Hansen, A.; Neese, F. Natural Triple Excitations in Local Coupled Cluster Calculations with Pair Natural Orbitals. *J. Chem. Phys.* **2013**, *139*, 134101−134113.
(45) Kruse, H.; Grimme, S. A Geometrical Correction for the Inter- and Intra-Molecular Basis Set Superposition Error in Hartree-Fock and Density Functional Theory Calculations for Large Systems. *J. Chem. Phys.* **2012**, *136*, 154101−154116.
(46) Widegren, J. A.; Finke, R. G. A Review of the Problem of Distinguishing True Homogeneous Catalysis from Soluble or Other Metal-Particle Heterogeneous Catalysis under Reducing Conditions. *J. Mol. Catal. A: Chem.* **2003**, *198*, 317−341.
(47) Martínez-Calvo, M.; Couceiro, J. R.; Destito, P.; Rodríguez, J.; Mosquera, J.; Mascareñas, J. L. Intracellular Deprotection Reactions Mediated by Palladium Complexes Equipped with Designed Phosphine Ligands. *ACS Catal.* **2018**, *8*, 6055−6061.



DOI: 10.1021/acscatal.9b00210
*ACS Catal.* 2019, 9, 3792−3799